International Journal of Plasticity 114 (2019) 161–173

Contents lists available at ScienceDirect

International Journal of Plasticity

journal homepage: www.elsevier.com/locate/ijplas

Probing the phase transformation and dislocation evolution in dual-phase high-entropy alloys

Qihong Fang[a], Yang Chen[a], Jia Li[a,*], Chao Jiang[a,**], Bin Liu[b], Yong Liu[b], Peter K. Liaw[c,***]

[a] State Key Laboratory of Advanced Design and Manufacturing for Vehicle Body, Hunan University, Changsha, 410082, PR China
[b] State Key Laboratory of Powder Metallurgy, Central South University, Changsha, 410083, PR China
[c] Department of Materials Science and Engineering, The University of Tennessee, Knoxville, TN, 37996, USA

ARTICLE INFO

Keywords:
High-entropy alloys
Dual phase
Atomistic simulations
Associated deformation
Phase transformation

ABSTRACT

Some high-entropy alloys, which contain two or more component phases with highly different properties, can achieve an outstanding combination of high strength and high ductility, and even break in the strength-ductility trade-off. However, a detailed atomic-scale mechanism of the dynamic continuous microstructural evolution has not hitherto been performed, to limit the achievement of bulk dual-phase high-entropy alloys with the improved strength and toughness. Here we report the deformation and plasticity as well as strength in the dual-phase nanocrystalline high-entropy alloys with a variable volume fraction of face-centered-cube (FCC) and hexagonal closed-packed (HCP) phases using atomistic simulations during the tensile-straining tests. The results show that the amplitudes of additional interaction stresses and strains rely on such factors as the differences in the mechanical property and volume fraction of each phase. Due to the complexity of the phase and phase boundary, the mechanical properties of the dual-phase nanocrystalline high-entropy alloys, in general, cannot be accurately estimated on the basis of the simple mixed laws, which are dependent upon the volume fraction and yielding strength of individual phase. The aim of this study is to describe how the phase volume fractions affect the mechanical properties in the dual-phase high-entropy alloys. The flow stress and work hardening of the dual-phase high-entropy alloys can be explained on the basis of the mobile dislocation density and dislocation-induced phase transformation in the corresponding phases. The HCP-based high-entropy alloys show the good plasticity and high strength, and are unlike traditional alloys with the low ductility, owing to the occurrence of the HCP to FCC phase transformation. The strength of the dual-phase high-entropy alloy with the 16.7% FCC-phase volume fraction exceeds that of HCP-based or FCC-based matrix, due to the stronger interface hardening. We expect that these results would be helpful for designing and selecting dual-phase high-entropy alloys with great strength and good ductility in various engineering applications.

---

[*] Corresponding author.
[**] Corresponding author.
[***] Corresponding author.

E-mail addresses: lijia123@hnu.edu.cn (J. Li), jiangc@hnu.edu.cn (C. Jiang), pliaw@utk.edu (P.K. Liaw).

https://doi.org/10.1016/j.ijplas.2018.10.014
Received 19 July 2018; Received in revised form 23 October 2018; Accepted 31 October 2018

1. Introduction

A large number of dual-phase alloys, consisting of two ductile phases, have been regarded as the technologically-important materials due to the outstanding mechanical properties of these alloys (Wu et al., 2017; Kim et al., 2015; Li and Lu, 2017; Chen et al., 2016; Xu et al., 2015; Zhang et al., 2014). Examples of dual-phase alloys include two-phase titanium alloys, two-phase steels, and two-phase copper alloys amongst others (Lee et al., 2009; Kadkhodapour et al., 2011; Kim et al., 2012; Ramazani et al., 2013; Jha et al., 2015; Xie et al., 2009; Han et al., 2017; Ghassemi-Armaki et al., 2014), which can produce the solid-phase-transformation-induced plasticity (Norfleet et al., 2009; Fischlschweiger et al., 2012; Javanbakht and Levitas, 2015, 2016; Mahnken et al., 2012; Baxevanis et al., 2013; Levitas and Javanbakht, 2015a, b; Yu et al., 2018). Recently, the new-system high-entropy alloys (HEAs) (Yeh et al., 2004; Feng et al., 2017; Ding et al., 2018; Wu et al., 2018), containing two solid-solution phases (Abuzaid and Sehitoglu, 2018; Bönisch et al., 2018), are developed. The dual-phase HEAs have the high hardness up to 835 HV, and the high yielding strength up to 2.2 GPa (Li et al., 2016; Niu et al., 2018; Song et al., 2018), which exceed most of the data reported in the traditional dual-phase alloys. To date, the deformation and strengthening mechanisms in the dual-phase nanocrystalline HEAs still remain elusive at nanoscale.

In past several years, the amount of work has been tried to uncover the origin of combinations of high strength and good ductility in the dual-phase alloys. As well known, for the dual-phase alloys subjected to the loading, the plastic deformation always occurs in the softer phase. Either elastic only or plastic deformation takes place in the harder phase, which is dependent on the property and microstructure of each phase under the loading (Huang et al., 2016; Alekseeva et al., 2017; Svanidze et al., 2016). In many cases, the strain and stress differences between the constituent phases cause the good mechanical properties, attributed to a synergistic interaction of each phase (Wang et al., 2015). The high local stress and strain hardening happen, owing to the individual-phase-induced plastic incompatibility. This trend causes the premature fracture driven by the initiation and propagation of nanovoids. Based on the dislocation-dominated hardening theory, the strain hardening from each phase has been determined (Lu et al., 2009), to deal with the strengthening and deformation mechanisms in some dual-phase alloys. To further reveal the origin of their high strength and good plasticity, the crystal plasticity models and atomic simulations have been developed in the several decades (Tasan et al., 2014; Wu et al., 2017; Zheng et al., 2018). Using the crystal plasticity modeling, dislocation transmission through α/β phase boundaries in Ti alloys, and the connections between the observed strain and damage heterogeneity are carried out, which is beneficial to understanding deeply the dislocation-governed deformation mechanisms in the dual-phase alloys. In comparison with the traditional dual-phase alloys, the dual-phase HEAs have been shown to be a considerable potential for the demanding and advanced structural applications, by achieving the further enhancement in the strength-ductility balance (Tang et al., 2015; Zheng et al., 2013). Some previous work shows that the dual-phase HEAs might have a more attractive combination of outstanding mechanical properties than the traditional alloy systems (Li et al., 2016; Niu et al., 2018; Song et al., 2018; Tang et al., 2015; Zheng et al., 2013). The strain-induced transformation from the FCC to HCP phase and the dynamic-strain partitioning behavior are revealed in the dual-phase HEAs. As the HCP-phase fraction increases, the strength and ductility of the dual-phase HEA increase at higher local strain larger than 30% (Li et al., 2017b). As the volume fraction of the FCC phase increases from 31.5 to 67.8 at.% in the dual-phase HEA, the compressive fracture strain increases from 14.9% to 29.9%, but the compressive strength and yield strength decrease from 1961.2 to 1380 MPa and from 1702.8–899.8 MPa (Guo et al., 2018). Lately, the simultaneously increased strength and ductility can be realized by the grain refinement in the dual-phase HEA with the total elongation of 75% and the ultimate tensile strength of 800 MPa, owing to the dynamic forward transformation from the FCC into HCP structure and the dynamic reverse transformation from the HCP into FCC structure at room temperature (Lu et al., 2018).

The previous experiment shows that the as-milled CoCrFeNiMn HEAs are constituted of the FCC and BCC phases with an average grain size of about 12 nm, and exhibit a high compressive strength of 1987 MPa at room temperature (Ji et al., 2015). Recently, the thermodynamic properties of the prototype equi-atomic CoCrFeMnNi HEAs are investigated, using finite-temperature ab initio methods (Li et al., 2017a; Gao et al., 2016; Ma et al., 2015), revealing that the HCP phase is the stable phase, and the BCC phase is the most unstable phase in the CoCrFeNiMn HEA. In order to promote the effective crystal engineering development, the understanding of the structure-property relationship in metals and alloys has a very important role in the development of the desired product performance.

In the present work, the relationships between the micromechanism and the associated deformation behavior are studied by the molecular dynamics (MD) simulations. Considering the effect of the highly inhomogeneous internal stresses, MD simulations are capable of elucidating the real-time behavior about the microstructure evolution and interaction during the deformation, which are extremely difficult observed by experimental techniques. Compared to the experimental investigation, MD simulations have several advantages for studying the atomic-level deformation mechanisms of nanocrystalline materials in a degree of details that cannot be obtained experimentally (Zhu et al., 2012). Moreover, we have investigated the contribution of each phase to the dislocation evolution and deformation in the dual-phase CoCrFeNiMn HEAs, in general. What's more, the microstructural evolution of each phase reveals the effects of the HCP to FCC phase transformation and the various types of dislocations on the strength and the associated deformation behavior in dual-phase HEAs.

2. Methods and models

The nanocrystalline dual-phase CoCrFeMnNi HEAs have the average grain size of 12 nm, and contains 6 grains built by the Voronoi methods, presented in Fig. 1a. The orientation of grain 1 is x-[100], y-[010], and z-[001]; that of grain 2 is x-[121], y-[10-1], and z-[1-11]; that of grain 3 is x-[11-1], y-[112], and z-[1-10]; that of grain 4 is x-[110], y-[1-10], and z-[001]; that of grain 5 is x-

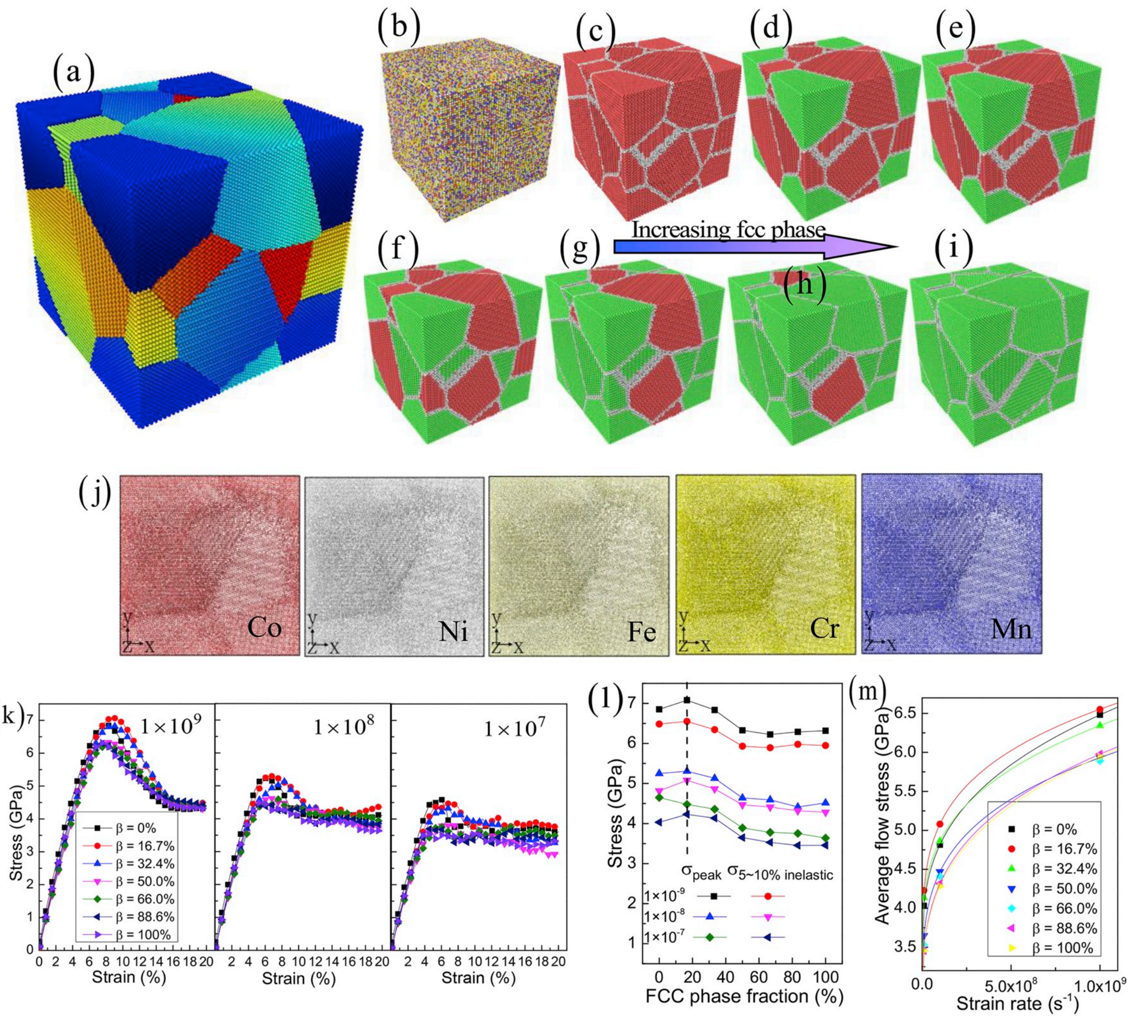

Fig. 1. The models of the dual-phase nanocrystalline CoCrFeMnNi HEA are colored according to the phase volume value (a), and the element type (b). In (b), ● Co, ● Ni, ● Fe, ○ Cr, and ● Mn. The FCC phase volume fraction, β, includes 0% (c), 16.7% (d), 32.4% (e), 50.0% (f), 66.0% (g), 88.6% (h) and 100% (i), where β is the volume fraction between the FCC-phase volume and the matrix volume in the dual-phase HEA. Here, $\beta = 0\%$ represents the HCP-phase CoCrFeMnNi HEA, $\beta = 100\%$ represents the FCC-phase CoCrFeMnNi HEA, and $0\% < \beta < 100\%$ represents the dual-phase CoCrFeMnNi HEA. In (c-i), ● face-centered-cubic (FCC), ○ unknown, ● hexagonal-close-packed (HCP), and ● body-centered-cubic (BCC). (j) The z-axis projection views of the distributions of various type atoms in the HEA. (k) Stress-strain relationship for different FCC-phase volume fractions and strain rates. (l) Variations in the yielding stress and average flow stress plotted as a function of the FCC-phase fraction at different strain rates in the dual-phase FeCoCrNiMn HEA. (m) Variations of the average flow stress and strain rate, and the corresponding fitting curves.

[031], y-[0-13], and z-[100]; and that of grain 6 is x-[0-13], y-[100], and z-[031]. The orientation of each grain is different along the x direction to meet the reasonable structure of the nanocrystalline HEA. In the MD model, the type of every atom is randomly selected until the targeted composition, which agrees with the given elemental composition from the previous experimental report (Ji et al., 2015), is obtained (Fig. 1b). The lattice constants of the FCC and HCP phases are 3.593 Å and 2.5 Å, which are measured by the X-ray diffractometer pattern in the experiment and the first principles calculation (Bhattacharjee et al., 2014; Ji et al., 2015; Widom et al., 2016). The size of the MD sample with approximately 542,000 atoms is $18.5 \times 18.5 \times 18.5\,\text{nm}^3$. A second nearest-neighbor modified embedded-atom method (2NN MEAM) potential (Choi et al., 2018) is described for the interactions of atoms in the nanocrystalline HEA, and this potential can clarify the fundamental reasons for sluggish diffusion and solid-solution hardening. All directions are described in periodic boundary conditions. The temperature is 300 K during the MD simulations. The time step of atomic simulations is set to 1 fs.

The equilibrium configurations can be achieved by the two steps, as follows: firstly, the system of the nanocrystalline dual-phase CoCrFeMnNi HEA is applied to the NVT dynamics at 300 K for 100 ps, and then the NPT dynamics at 300 K for 300 ps for relaxing the system and alleviating the out-of-balance forces and net stresses. The system of nanocrystalline dual-phase CoCrFeMnNi HEA is subjected to the applied strain rates between 1×10^7 and $1 \times 10^9\ \text{s}^{-1}$ along the x direction under the NPT ensemble with a zero-pressure condition, to investigate the strain rate effect on the deformation behavior. Now, the experiments of femtosecond laser driven shocks can obtain the high strain rate in the range of 10^7 - 10^9 s^{-1} (Crowhurst et al., 2014). The MD simulations are implemented with the open-source, LAMMPS (Plimpton, 1993). The open-source software, Ovito (Stukowski, 2012), is employed for visualizing the evolution of the atomistic structure. The common-neighbor analysis (CNA) method is used to identify the local atomic structures, where green atoms represent the FCC structure, blue atoms indicate the BCC structure, red atoms are stacking faults, and white atoms stand for grain boundaries or dislocation cores.

Using standard straining methods, the elastic constants of C11, C12 and C44 for the FCC CoCrFeMnNi HEA are determined, yielding C11 = 264.6 GPa, C12 = 184.8 GPa, and C44 = 112.9 GPa. Here, the expression of the Young's modulus is $E = 9BG/(3B + G)$ (Hill, 1952; Landau and Lifshitz, 1999), where $B = (C_{11} + 2C_{12})/3$, $G = (G_V + G_R)/2$, $G_V = (C_{11} - C_{12} + 3C_{44})/5$, and $G_R = 5(C_{11} - C_{12})C_{44}/[4C_{44} + 3(C_{11} - C_{12})]$. Hence, the Young's modulus obtained from the MD simulation is 199.9 GPa with 9% error, compared to the previous experimental data of 220 GPa (Li and Raabe, 2017). The anisotropy ratio, $\alpha = 2C_{44}/(C_{11} - C_{12})$, represents the elastic anisotropy of a material. Here, the anisotropy ratio of the single-crystal CoCrFeMnNi HEA is 2.83. The anisotropy ratio of the nanocrystalline HEA is 1.09, and very close to 1.0 compared to that of single crystal FCC HEA. It demonstrates the elastic isotropy of the built nanocrystalline HEA, attributed to the random orientations of the grains.

3. Results

To investigate the effect of the FCC-phase volume fraction on the mechanical properties and the associated deformation behavior in the dual-phase nanocrystalline CoCrFeMnNi HEA (Fig. 1a), a series of MD models are created in Fig. 1c-i, where the FCC-phase volume fraction changes from 0% to 100%. The z-axis projection views of the different element distributions show the compositional distribution among the five elements in nanocrystalline CoCrFeMnNi HEA (Fig. 1j). No apparent elemental segregations observed in the CoCrFeMnNi HEA reveal the uniform distribution in the various types of atoms. Similarly, the nanoscale chemical elemental distribution can be characterized by means of scanning transmission electron microscopy coupled with atom probe tomography in the CoCrFeMnNi HEA (Li et al., 2017b; Santodonato et al., 2015; Lu et al., 2018).

The corresponding stress-strain curves show that the values of elastic modulus are dependent upon the phase-volume fraction, indicating that the HCP HEAs have higher elastic modulus than the FCC HEAs. Compared with the classical HCP-based nanocrystalline alloys, the work hardening and tensile ductility are simultaneously improved in the HCP-based nanocrystalline HEAs (Fig. 1k and l). This result is unlike the conventional understanding that the brittle HCP phases improve the yielding strength, but reduce the ductility. The peak and average flow stresses increase with the decreasing FCC phase, attributed to the increased hard HCP phase. As shown in Fig. 1l, the dual-phase HEA with a low FCC phase fraction of about 16.7% has not only higher strength, but also good plasticity, agreeing with the previous reports (Li et al., 2016; Li and Raabe, 2017).

As well-known, MD simulations due to the short time duration always involve extremely high strain rates (of typically larger than 10^7 s^{-1}), which are much higher than in the conventional tensile/compressive experiments. Compared with experimental results, the MD simulations are more complex due to the fact that the strain rate has a significant effect on the deformation mechanisms. For example, it is generally agreed that higher strain rates promote the deformation twinning in nanocrystalline materials (Zhu et al., 2012). Recently, the yield transition of metal nanowires occurs from the nucleation of Shockley partials on primary slip systems at MD strain rates more than 10^7 s^{-1} to the nucleation of planar defects on non-Schmid slip planes at experimental strain rates less than 10^{-2} s^{-1} (Tao et al., 2018). The high deformation stresses under high strain rates are not entirely unusual in experimental studies of nanocrystalline materials. For instance, in the recent experiments, the dislocations nucleate simultaneously from multiple sources at the estimated shear stress of 7.2 GPa on the (101) slip plane in the bicrystal tungsten (Wang et al., 2015). The onset of plasticity in the nanocrystalline NiTi with the grain size of 50–100 nm is visible at a stress of about 2.4 GPa (Ghassemi-Armaki et al., 2017), and the dislocations nucleate and propagate in the nanocrystalline Ni_3Al with a grain size of 50 nm at a stress of 1.5 GPa (Yamakov et al., 2004). These values of stresses from the experiments are very similar to the values of typical stresses from the MD simulations. Hence, from the perspective of deformation mechanisms, the higher strain rate in the FeCoCrNiMn HEA could greatly result in the formation of deformation twinning, compared to the low strain rate. From the viewpoint of mechanical properties, the higher strain rate leads to a higher yielding strength of the dual-phase nanocrystalline FeCoCrNiMn HEA. In the previous work (Tao et al., 2018), the yield stress at high strain rate of 10^{10} s^{-1} has 2 times higher than that at the low strain rate of 10^{-3} s^{-1} in the bicrystalline nanowires. Here, the average flow stress declines rapidly with the decrease of the strain rate from 1×10^9 to 1×10^8 s^{-1}, but it declines slowly with the decrease of the strain rate from 1×10^8 to 1×10^7 s^{-1} (Fig. 1k and l). As a result, the average flow stress goes down 37% from 1×10^9 to 1×10^7 s^{-1}. The previous work (Cowper and Symonds, 1957) can show the strain-rate dependence of the average flow stress using a power function relationship of $\sigma_y = a + b\dot{\varepsilon}^c$, where σ_y is the average flow stress, $\dot{\varepsilon}$ is the strain rate, and a,b,c are the fitting parameters of the strain-rate sensitivity. The fitting parameters in the different phase volume fractions can be described in Table 1. The corresponding fitting curves for the relation between the mechanical property and strain rate are shown in Fig. 1m,

Table 1
The fitting parameters of the dual-phase HEAs with various phase volume fractions under different strain rates.

Parameters Phase fractions	0	16.7%	32.4%	50.0%	66.0%	88.6%	100%
a	3.338	3.06	3.427	2.606	2.233	2.524	2.642
b	3.503×10^{-3}	2.53×10^{-2}	4.982×10^{-3}	1.802×10^{-2}	3.428×10^{-2}	9.46×10^{-3}	6.02×10^{-3}
c	0.3281	0.2378	0.3075	0.2518	0.2254	0.2847	0.3044

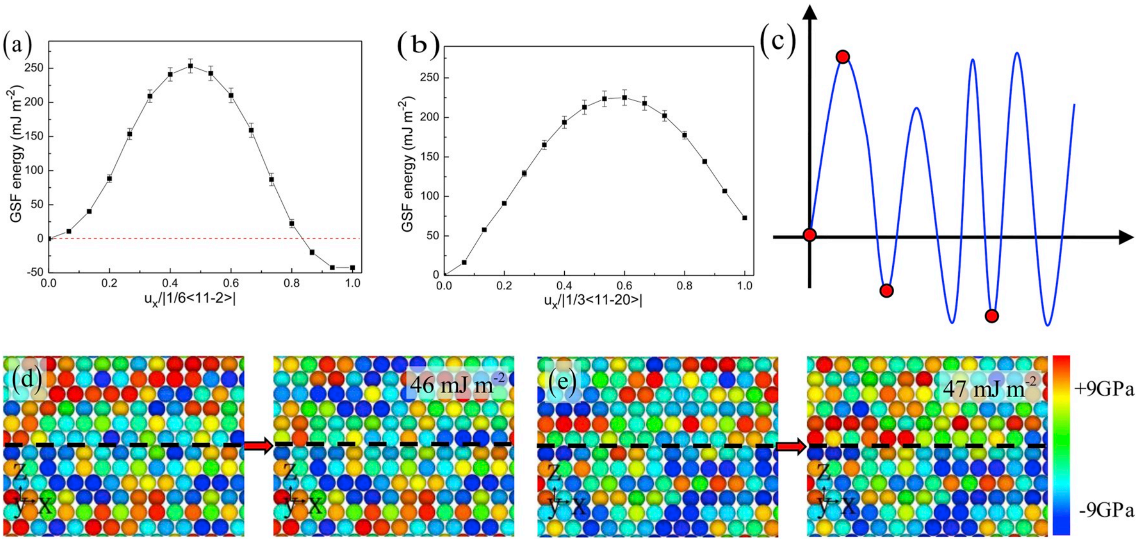

Fig. 2. (a) Generalized-stacking-fault (GSF) energy for the [11-2](111) slip system in the FCC phase, and (b) GSF energy for the [11-20](0 0 0 1) slip system in the HCP phase of the FeCoCrNiMn HEA. Error bars (± standard deviation) represent the fluctuation of the GSF energy induced by the random distribution of the alloying elements. (c) the stress distribution along the moving direction between upper and lower layers. The atomic distance changes at every layer when atoms move. (d, e) the stress distribution of the initial state and stacking fault state for the two different atomic configurations built by the random distribution of various elements.

where the value of the average flow stress at a quasistatic state ($\dot{\varepsilon} \rightarrow 0$) can be obtained and considered to equal to the fitting parameter, a, based on the power function relationship.

The stacking fault energy (SFE) of metals and alloys controls frequently the deformation mechanisms, including the dislocation slipping, and deformation twinning, as well as phase transformation (Wang et al., 2018). For example, for SFE > $45\,\mathrm{mJ\,m^{-2}}$, the dislocation slip dominates the plasticity and strain hardening of alloys (Grässel et al., 2000); for SFE between 18 and $45\,\mathrm{mJ\,m^{-2}}$, deformation twinning governs the plastic behavior (Wang et al., 2018); for SFE $< 18\,\mathrm{mJ\,m^{-2}}$, martensitic transformation from the FCC to HCP phase takes place, managing the plastic deformation (Curtze and Kuokkala, 2010). Here, SFE for the FCC CoCrFeMnNi HEA is - $49\,\mathrm{mJ\,m^{-2}}$ in accordance with the previous studies (Zhang et al., 2017a; Zhao et al., 2017) (Fig. 2a), leading to that the partial dislocations are more likely to occur, compared to the full dislocation. The SFE for the HCP CoCrFeMnNi HEA is $72\,\mathrm{mJ\,m^{-2}}$ (Fig. 2b), indicating that the nucleations of dislocations are more likely to occur in the FCC phase, compared to the high SFE in HCP phase. Moreover, based on the energy differences, the HCP phase may be more stable than the FCC phase at 300 K, agreeing with the results of the first principles calculations (Huang et al., 2018). The local stress field induced by the atomic-level severe lattice distortion causes the fluctuation of SFE, owing to the random distribution of elements with various atom sizes (see Fig. 2a and b) (Liu and Wei, 2017; Li et al., 2018). The upper atom layer moves, resulting in the stress redistribution (see Fig. 2c–e). The high stress region is located in the middle layer, causing the high SFE (see Fig. 2d and e). In addition, the difference of the atomic interlayer spacing induced by the disorder could lead to the difference of SFE, due to the chemical inhomogeneities of HEAs.

After the tension deformation at a strain of 20%, the volume fractions of different microstructures in the dual-phase HEA are shown in Fig. 3a. As the volume fraction of the FCC phase increases, the volume fractions of other structures, including dislocations and grain boundaries, firstly increase and then drop, confirming the phase and grain-boundary effect on the associated deformation (see, structural evolution of Fig. 3b–g). Interestingly, after the plastic deformation, the FCC phase is accounted for about 10% in the HCP-based FeCoCrNiMn HEA, indicating the occurrence of phase transformation from the HCP to FCC phase (Fig. 3a). Recently, the HCP to FCC phase transformation in the polycrystalline CoCrFeMnNi HEA is observed by in situ laser/resistive heating XRD experiments (Zhang et al., 2017b), and during depressurization (Tracy et al., 2017), attributed to the metastable HCP phase. In addition, the crystalline lattices of HCP and FCC phases are very closely attributed to their inner energy with the relatively small barrier for the HCP to FCC transformation, and vice versa (Huang et al., 2018; Zhang et al., 2017b; Pogrebnjak et al., 2016). To further confirm the microstructure evolution of the nanocrystalline dual-phase HEA during plastic deformation, the fraction of each structure varies with the increased strain (Fig. 2h). For the strain larger than 5%, the FCC phase in the dual-phase HEA decreases, but the HCP phase increases in the dual-phase HEA with the HCP phase less than 50%.

The phase-transformation processes firstly from the HCP to FCC phase, and then from the FCC to HCP phase are depicted in detail, as shown in Fig. 4. The dislocation nucleated from the grain boundary is emitted to the grain interior, and the adjacent dislocation moves along the reverse direction (Fig. 4b). The newly nucleated dislocation continuously slips towards the opposite grain boundary (Fig. 4c), resulting in the formation of the FCC structure with the six-atomic-layer thicknesses. As the applied strain increases, the partial dislocation emitted along the slip plane creates a stacking fault in the newly nucleated FCC phase (Fig. 4d–f), meaning the occurrence of reverse phase transformation from the FCC to HCP structure. The process of the HCP to FCC phase transformation can improve the plasticity of the HCP FeCoCrNiMn HEA (Li et al., 2016), attributed to that phase transformation induces the structure

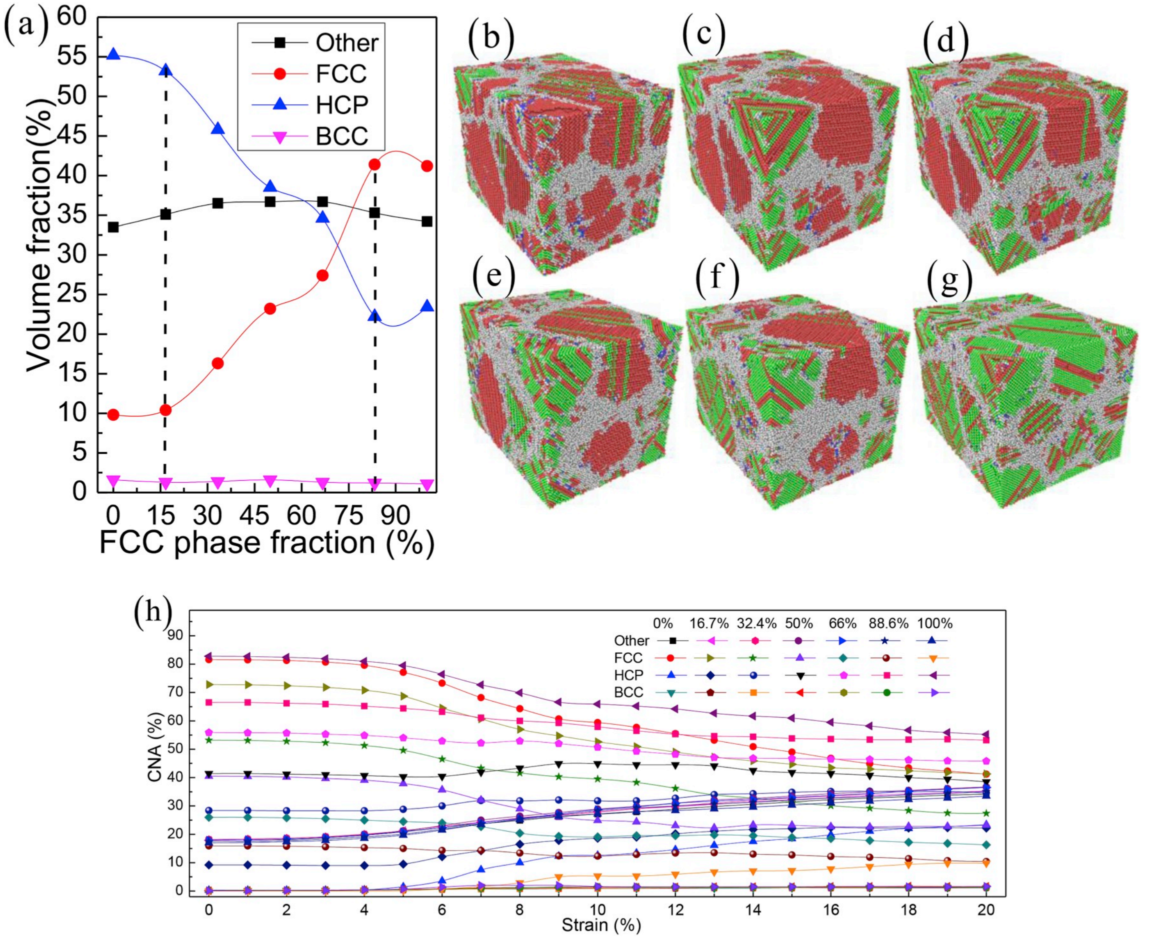

Fig. 3. Volume fraction of the microstructures with the increasing FCC phase (a), and the corresponding structural evolution of the FeCoCrNiMn HEA (b-g) at a strain of 20%. Evolution of the fractional phase content with the increasing strain (h).

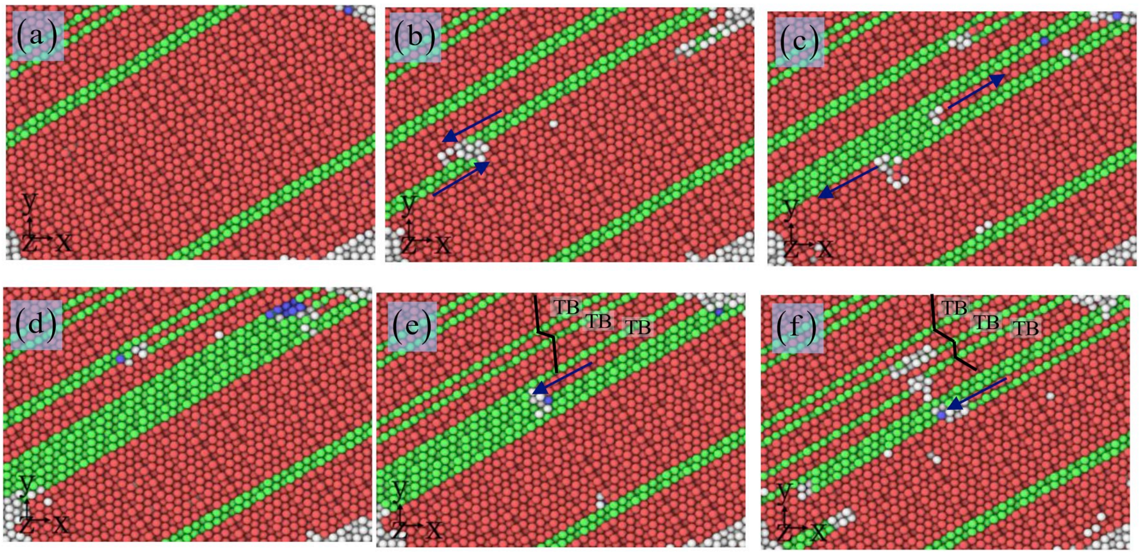

Fig. 4. The HCP to FCC phase transformations of the HEA (a-d), and the FCC to HCP phase transformations of the HEA (d-f) by the dislocation slipping. The arrows indicate the movement direction of the partial dislocation. 'TB' represents the boundary of deformation twinning.

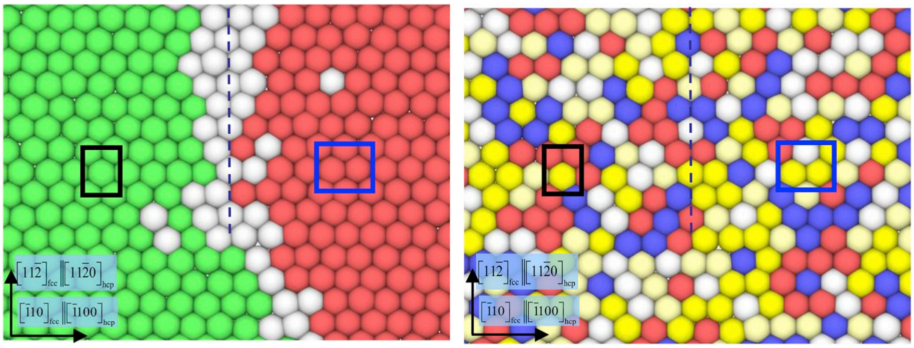

Fig. 5. The transformation from the HCP to FCC phase at the strain of 5%.

dissipation, and the new-generated FCC phase has more slip systems. In addition, the formation process of deformation twinning is observed during the phase-transformation process (Fig. 4 e,f), which is created by the motion of the partial dislocations.

The transformation from the FCC crystal structure (ABCABC… stacking sequence) to the HCP crystal structure (ABABAB… stacking sequence), and vice versa, can take place by the motion of the Shockley partial dislocations with Burgers vectors of type 1/6 < 11 -2 > on every second closest packed plane (Olson and Cohen, 1976). The phase transformation meets the orientation relationship, namely (111)FCC || (0001)HCP and [11-2]FCC || [11-20]HCP orientation (see Fig. 5), forming the coherent phase interfaces (Fig. 5a). Hence, the FCC→HCP phase transformation can be realized by the dissociation of the perfect dislocations and the HCP→FCC phase transformation by the association of the Shockley partial dislocations (see Fig. 5). In other word, the "back and forth" movement of the same Shockley partial dislocations occurs, resulting in the reversible HCP→FCC transformation with the preservation of the orientation. This prediction is in good agreement with a previous experimental result investigated in the dual-phase HEA (Lu et al., 2018).

Fig. 6 shows the formation process of deformation twinning with the increasing strain in the FCC phase. The twinning partial dislocation is nucleated (Fig. 6b, g), and moved in the opposite direction, resulting in the increased thickness in the deformation twinning region. The full dislocation is nucleated in the stacking fault region (Fig. 6c, h), and then can be dissociated into two partial dislocations. As the strain increases, the two partial dislocations can move along the opposite directions, causing the continuous increase of the deformation twinning (Fig. 6e, j), and agreeing with the previous experimental report (Wang et al., 2015).

Furthermore, the dual-phase HEA with a 16.7% FCC phase has the higher strength (Fig. 1k), originated in the phase interface hardening, which is proved by increasing the other structure volume fraction in Fig. 3a. During the initial strain phase, the FCC phase undergoes the plastic deformation and the HCP phase undergoes the elastic deformation. Then, the HCP phase begins to deform plastically until the FCC phase achieves a certain degree of strain hardening. When the volume fraction of the FCC phase is larger than 15%, the hard HCP phase decreases sharply, and the interface strengthening weakens (Fig. 3a), resulting in the decrease in the flow stress (Fig. 1k). The existence of the grain boundary in the FCC phase can lead to the softening with the increase of the FCC phase, which exceeds the contribution of the phase-interface hardening relying on the dual-phase crystallographic orientation. In addition, the dislocation hardening and deformation twinning also play a key role in the flow stress (Figs. 4 and 6).

To understand the relationship between the dislocation evolutions and material properties in the dual-phase HEA, the change trend of the dislocation density with the increasing strain is presented in Figs. 7 and 8 for different FCC phase fractions. The dislocation density can be defined as the ratio of the sum of all the dislocation lengths and the volume of the dual-phase HEA. The plasticity of metals and alloys depends on the microstructural evolutions, such as the dislocation motion, kinking, twinning, slip, and lattice instability (Khan et al., 2011; Li et al., 2010; Yu et al., 2010; Zhu et al., 2012; Wang et al., 2017). Here, the dual-phase

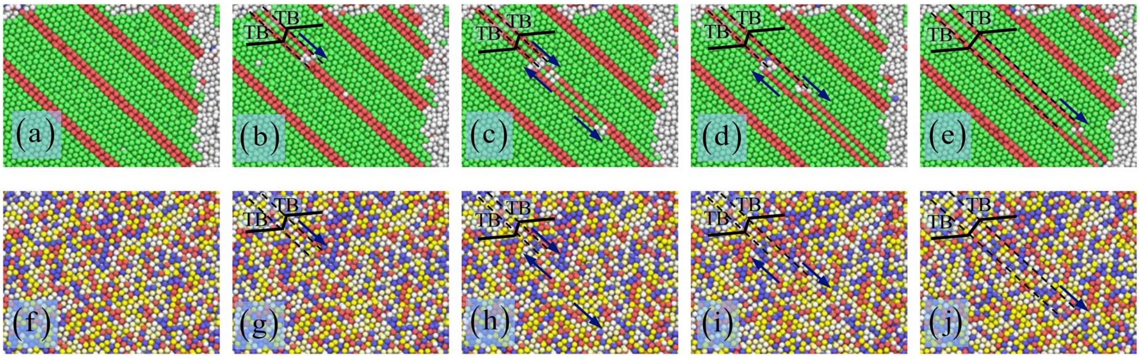

Fig. 6. The deformation twinning process at the strain: 5% (a, f), 6% (b, g), 7% (c, h), 9% (d, i), and 10% (e, j). The atoms are colored according to the CNA value in (a-e), and the atom type in (f-j).

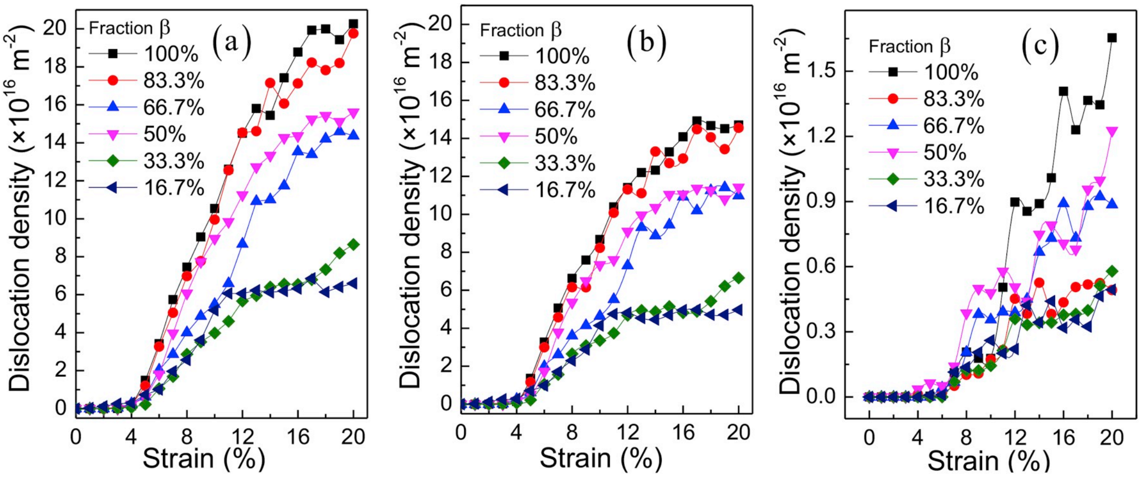

Fig. 7. Evolution of dislocation density, Shockley partial dislocation density, and stair-rod dislocation density in the FCC phase.

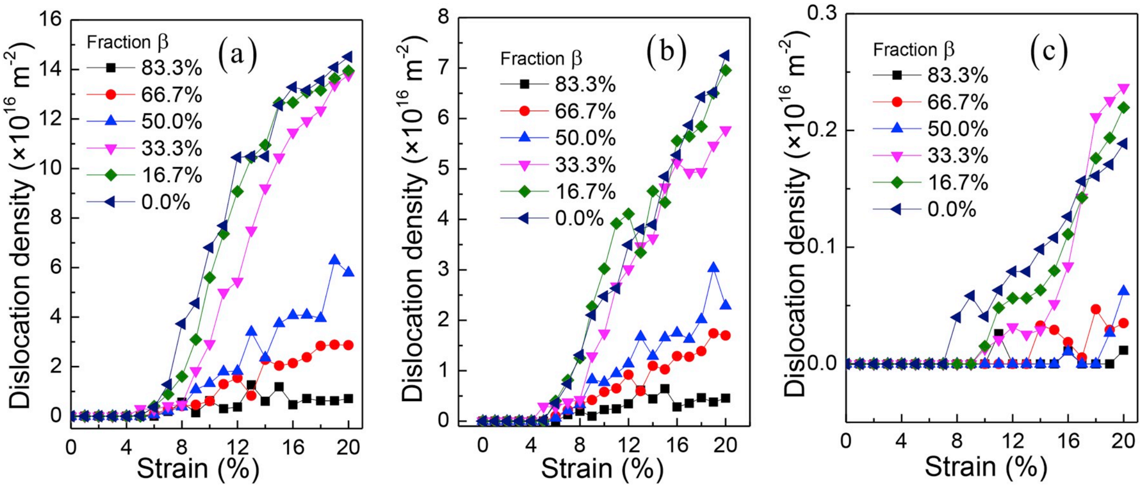

Fig. 8. Evolution of dislocation density, the 1/3 < 1-100 > dislocation density, and 1/3 < 1-210 > dislocation density in the HCP phase.

CoCrFeMnNi HEA has the low SFE, which is easier to drive the partial dislocation motion and the phase transformation. In the dual-phase HEA, the dislocation motions through the regions with the lattice-distortion-induced complex stresses lead to the crystal plasticity, where the unexpected stress in slip planes appears in a given crystallographic crystal (Cubuk et al., 2017), and is associated with the high strength of the HEA. In Fig. 7, a large number of Shockley partial dislocations to slip in the < 111 > plane give rise to the very high plasticity in the FCC phase. The interaction between the nucleated partial dislocations can result in the stress dependence, owing to the formation of stair-rod dislocations (Barnard et al., 2006). Therefore, the increasing Shockley partial dislocation density can improve the plasticity, and the increasing stair-rod dislocation density can enhance the strength in the FCC phase. The FCC HEAs have a higher dislocation density than the HCP HEAs, due to the more slip systems activated (Figs. 7 and 8). Hence, with the increasing strain, the mobile dislocation density increases to cause the high plasticity of the HEA, and the sessile dislocation density increases to improve the high strength of the HEA (Li et al., 2016). This trend can explain why such a dual-phase HEA with a 16.7% FCC phase have a high strength and good plasticity, compared with that of the HCP HEA and other dual-phase HEA. It is due to that the high mobile and sessile dislocation densities resulting from the phase-interface interaction are observed in the dual-phase HEA with a 16.7% FCC phase (Figs. 7 and 8). As a result, the total dislocation densities in this dual-phase HEA are greater than that in the HCP-based HEA, yielding the good ductility; the sessile dislocation densities of the unit FCC-phase volume in this dual-phase HEA are higher than that in the other dual-phase HEA, leading to the high strength. Thus, in the dual-phase HEAs, introducing the more slip planes plays a key role in improving the plasticity, and introducing a certain number of phase boundaries is a valid strategy for the strength enhancement.

4. Discussion

The structure of the present dual-phase HEA generally consists of the FCC and HCP phases. At any given strain in the plastic range, the mean flow stress needed for overall straining of the dual-phase HEA can be described by the rule of mixture (Ankem et al., 2006)

$$\sigma = V_{fcc}\sigma_{fcc} + V_{hcp}\sigma_{hcp} + I_{fcc-hcp} \tag{1}$$

where V_{fcc} and V_{hcp} represent the volume fractions of the FCC and HCP phases, respectively, which meet the relationship of $V_{fcc} + V_{hcp} = 1$. σ_{fcc} and σ_{hcp} are the average in-situ stresses in the FCC and HCP phases per volume unit, respectively. $I_{fcc-hcp}$ is the interacting stress between the FCC and HCP phases, which could be positive or negative (Ankem et al., 2006; Maier-Kiener et al., 2017).

To reveal the strengthening model in the continuous FCC matrix HEA when the phase transformation from FCC to HCP phase occurs, the mean flow stress as a function of the volume fraction of the minor HCP phase can be described by modifying Eq. (1)

$$\sigma = \sigma_{fcc} + V_{hcp}(\sigma_{hcp} - \sigma_{fcc}) + I_{fcc-hcp} \tag{2}$$

For the continuous HCP matrix HEA when the phase transformation from HCP to FCC phase occurs, the mean flow stress as a function of the volume fraction of the minor FCC phase also can be expressed by modifying Eq. (1)

$$\sigma = \sigma_{hcp} + V_{fcc}(\sigma_{fcc} - \sigma_{hcp}) + I_{fcc-hcp} \tag{3}$$

Thus, the strength of the dual-phase HEA can be derived from the sum of three terms, which include the strength from the matrix phase, the discontinuous minor phase, and the phase interface between the matrix and minor phase. The second term depends on the minor phase volume fraction and the phase mechanical property difference, and the later term is controlled by the strong interaction of the FCC-HCP phase interface. In the present paper, Eqs. (2) and (3) can interpret the flow stress of the dual-phase HEA, and determine the strengthening contribution of the individual phase dependent upon its flow stress. The flow stress can be regarded as one of the most important mechanical-property parameters, which has a linear relationship with the volume fraction confirmed experimentally (Huang et al., 2016; Ankem et al., 2006). Beyond expectation, in the dual-phase HEA with a FCC-phase of 16.7%, the flow stress exceeds the FCC-based or HCP-based HEA matrix (Fig. 1), owing to the dislocation hardening, twinning hardening, and transformation-induced hardening from the interface (Li et al., 2016).

The tensile data of the FCC and HCP nanocrystalline HEAs indicates that the HCP HEA has a high flow stress (see Fig. 1j and k). As a result, the HCP-based HEA matrix is softened by the presence of the high FCC-phase volume fraction, meaning that the third term in Eq. (3) is negative. On the other hand, the FCC-based HEA matrix is strengthened due to the presence of the HCP phase, indicating that the third term in Eq. (2) is positive. In other words, the flow stress drop with the increasing FCC-phase volume fraction in the dual-phase HEA is attributed to the increasing volume fraction of the softer FCC phase at the expense of the stronger HCP phase. Apart from the volume fraction and the strength of each phase, the associated deformation behavior of the dual-phase HEA relies on the strong interface interaction and topology. If the dual-phase HEA constitutes of the continuous hard HCP matrix and the discontinuous soft FCC phase, overall straining agrees with that of the harder HCP phase. On the other hand, if the situation is the continuous soft FCC phase and the isolated hard HCP phase, the deformation process mainly takes place in the soft FCC phase (Barnard et al., 2006). These cases reveal that the overall straining behavior in dual-phase HEAs can largely depend on the straining properties of the matrix phase.

To further investigate the interface effect on the deformation and strength of the dual-phase HEAs, the microstructure evolution, the strain distribution, the stress distribution, and the dislocation evolution are shown in Fig. 9. Compared to the FCC HEAs, the thickness of the interface between the FCC and HCP grains obviously increases, resulting in the interface strengthening by increasing the inter-grain slip resistance (Li et al., 2016). When the HCP phase volume fraction is low, the HCP grains only deform elastically (Fig. 9 a1 and a2). With continuously increasing the HCP phase volume fraction, the HCP grains deform partly elastically and partly plastically, while the FCC grains deform plastically (Fig. 9 a3-a6). The small amount of the FCC phase can reduce the degree of the plastic deformation in comparison with the pure HCP HEAs. The grain or phase boundaries withstand the high strain arising from the large deformation (Fig. 9 b1-b6). The emitted partial dislocation with the stacking fault in the FCC grain, and the HCP to FCC phase transformation in the HCP grain store a large number of strain energy, coordinating to the large plastic deformation (Fig. 9 b1-b6). The dislocations included in the transforming grain could relax the stress concentrator, to reduce the driving force for phase transformation (Javanbakht and Levitas, 2015, 2016; Levitas and Javanbakht, 2015a, b). The stress distribution around grain and phase boundaries is shown in Fig. 9 c1-c6, revealing that the compressive stress fields occur at the regions of the grain and phase boundaries. Plasticity plays a dual part in the interaction with phase transformations. Dislocation pile-ups produce strong stress concentrators that lead to the barrierless phase nucleation. On the other hand, plasticity in the transforming grain relaxes the stress concentrator to suppress the phase nucleation (Javanbakht and Levitas, 2015, 2016; Levitas and Javanbakht, 2015a, b). The atomic severe lattice distortion induces the complex stress in the FCC and HCP grains, where the free-stress region takes place and is surrounded by high stress areas. This stress distribution affects the local stacking fault energies, which control the slip resistance and nucleation critical stress of the dislocation in the phase and grain boundary. Hence, the origin of interface strengthening or softening is dependent on the degree of the local chemical order in the dual-phase HEA (see, dislocation evolution in Fig. 9 d1-d6). Thus, it could help understand deeply the phase/grain boundary-property relationships to scientifically drive the development of new dual-phase HEA with targeted mechanical behavior.

In addition, a dual-phase nanocrystalline HEA is highly heterogeneous in terms of chemical compositions, grain structures, and grain-boundary networks, which together with the volume fractions of phases, all playing important roles in determining its mechanical performance. The current study mainly deals with the effect of the volume fraction of phases on the deformation behavior and mechanical properties. The remaining key factors left for future work, and beyond the scope of this study. To further improve the strength of HEAs, the third hard phase, such as the BCC phase or precipitates could be introduced in the dual-phase HEAs. It is due to

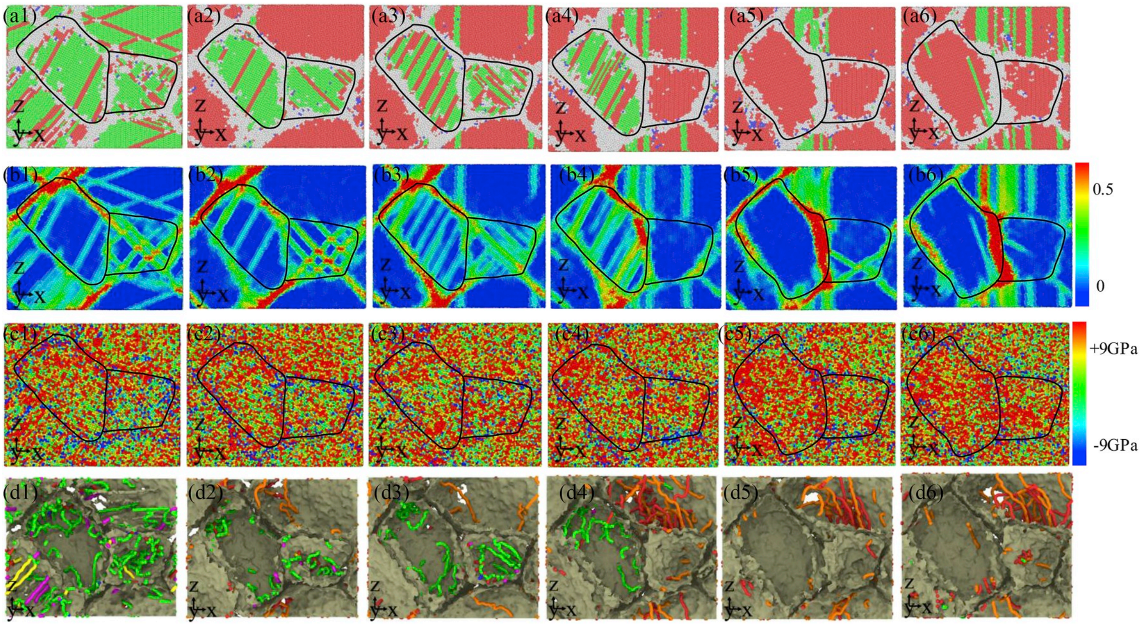

Fig. 9. The microstructures (a1-a6), the strain distributions (b1-b6), the stress distributions (c1-c6), and the dislocation configurations (d1-d6) at a strain of 14.0% and the FCC phase volume fractions: 100% (a), 66% (b), 50.0% (c), 33.3% (d), 16.7% (e), and 0% (f). In (b1-b6), the red atoms indicate the high strain region, and the blue atoms denote the low strain region. In (c1-c6), the red atoms indicate the high tensile stress region, the blue atoms denote the high compressive stress region, and the green atoms represent the low stress or stress-free region. In (d1-d6), as indicated by the line colors, dislocations, including perfect dislocations (— blue line), Shockley partials (— green line), Hirth (— light-yellow), and stair-rod (— pink line) dislocations, have nonstandard Burgers vectors in the FCC phase. The dislocations, including 1/3 < 1-210 > partials (— green line) and 1/3 < 1-100 > partials (— deep-yellow) dislocations, have nonstandard Burgers vectors in the HCP phase. (For interpretation of the references to color in this figure legend, the reader is referred to the Web version of this article.)

that the dislocation could cut, or loop (Fang et al., 2019), or pile up the phase interface between the matrix and third phase (nanoprecipitate), resulting in the multi-level enhancement mechanisms. Recently, this strategy to design the HEAs with high-content nanoprecipitates, greatly strengthens HEAs without severely losing ductility (Liang et al., 2018; Ming et al., 2018). Therefore, our results helpfully guide the design and optimization of HEA with the desired combinations of the mechanical properties, by tuning the proportions of different phases.

5. Conclusions

The deformation behaviors of the dual-phase nanocrystalline HEAs with variable fractions of FCC and HCP phases due to different heat treatments have been examined by the tensile straining test. We also investigate the FCC phase volume fraction on the mechanical properties and the associated deforming behaviors of the dual-phase nanocrystalline CoCrFeMnNi HEA. The HCP HEAs have higher elastic modulus compared to the FCC HEAs, indicating that the addition of the HCP phase initiates the hardening of the dual-phase HEA. The HCP nanocrystalline HEA has the high work hardening and good ductility, which is unlike conventional understanding of the brittle HCP phase with the high yielding strength and low ductility. Interestingly, the FCC phase is accounted for about 10% in the nanocrystalline HCP-phase FeCoCrNiMn HEA, indicating the occurrence of the HCP to FCC phase transformation. The HCP to FCC phase transformation and the reverse FCC to HCP phase transformation, which strongly correlates with the degree of the atomic lattice distortion, improve the plasticity of the HCP grain. With the increasing strain, the mobile dislocation density increases to cause the high plasticity of the HEA, and the sessile dislocation density increases to improve the high strength of the HEA. The overall straining behavior of the dual-phase HEAs can be largely influenced by straining properties of the matrix phase, due to the strong effect of the phase boundary and phase transformation. The present results on the microstructure evolution at the nanoscale provide a useful benchmark for further the science-based design of the new dual-phase HEAs with the high strength and ductility.

Future work can be undertaken to investigate the role of chemical compositions, grain structures, and grain-boundary networks on the microstructural evolution and the damage in dual-phase HEAs. The previous work studied by the experiments has shown a key link between the phase volume fraction and macroscopic mechanical response in dual-phase HEAs. However, the MD simulations outlined in current study could greatly contribute to the previous experimental results by providing the numerical evidence for the underlying phase transformation and dislocation as well as twinning mechanism. Furthermore, various deformation methods, including shear deformation, femtosecond laser driven shocks, nano-indentation, high-pressure torsion, and cyclic deformation, could further give the fundamental role of multi-phase in controlling the plasticity and ductility of HEAs, to tailor quantitatively the mechanical properties of HEA.

Acknowledgements

The authors would like to deeply appreciate the support from the Foundation for Innovative Research Groups of the National Natural Science Foundation of China (Grant No. 51621004), the NNSFC (11772122, 51871092, 51625404, 51771232, and 51671217), the Fundamental Research Funds for the Central Universities (531107051151), and the National Key Research and Development Program of China (2016YFB0700300). PKL would like to acknowledge the Department of Energy (DOE), Office of Fossil energy, National Energy Technology Laboratory (DE-FE-0011194) with the program manager, Dr. J. Mullen. PKL very much appreciates the support of the U.S. Army Research Office project (W911NF-13-1-0438) with the program managers, Dr. M.P. Bakas, Dr. D.M. Stepp, and Dr. S.N. Mathaudhu. PKL thanks the support the National Science Foundation (DMR-1611180 and 1809640) with the program directors, Drs G. Shiflet and D. Farkas. The authors are thankful for the computational resource provided by the TianHe-1 supercomputer at the National Supercomputer Center in Changsha, China.

Appendix A. Supplementary data

Supplementary data to this article can be found online at https://doi.org/10.1016/j.ijplas.2018.10.014.

References

Alekseeva, S., da Silva Fanta, A.B., Iandolo, B., Antosiewicz, T.J., Nugroho, F.A.A., Wagner, J.B., Langhammer, C., 2017. Grain boundary mediated hydriding phase transformations in individual polycrystalline metal nanoparticles. Nat. Commun. 8, 1084.

Abuzaid, W., Sehitoglu, H., 2018. Plastic strain partitioning in dual phase Al13CoCrFeNi high entropy alloy. Mater. Sci. Eng. 720, 238–247.

Ankem, S., Margolin, H., Greene, C.A., Neuberger, B.W., Oberson, P.G., 2006. Mechanical properties of alloys consisting of two ductile phases. Prog. Mater. Sci. 51, 632–709.

Barnard, J.S., Sharp, J., Tong, J.R., Midgley, P.A., 2006. High-resolution three-dimensional imaging of dislocations. Science 313 319-319.

Baxevanis, T., Parrinello, A.F., Lagoudas, D.C., 2013. On the fracture toughness enhancement due to stress-induced phase transformation in shape memory alloys. Int. J. Plast. 50, 158–169.

Bhattacharjee, P.P., Sathiaraj, G.D., Zaid, M., Gatti, J.R., Lee, C., Tsai, C.W., Yeh, J.W., 2014. Microstructure and texture evolution during annealing of equiatomic CoCrFeMnNi high-entropy alloy. J. Alloy. Comp. 587, 544–552.

Bönisch, M., Wu, Y., Sehitoglu, H., 2018. Twinning-induced strain hardening in dual-phase FeCoCrNiAl0.5 at room and cryogenic temperature. Sci. Rep. 8, 10663.

Chen, G., Peng, Y., Zheng, G., Qi, Z., Wang, M., Yu, H., Liu, C.T., 2016. Polysynthetic twinned TiAl single crystals for high-temperature applications. Nat. Mater. 15, 876.

Crowhurst, J.C., Reed, B.W., Armstrong, M.R., Radousky, H.B., Carter, J.A., Swift, D.C., Zaug, J.M., Minich, R.W., Teslich, N.E., Kumar, M., 2014. The $\alpha \rightarrow \varepsilon$ phase transition in iron at strain rates up to $10^9\ s^{-1}$. J. Appl. Phys. 115, 113506.

Curtze, S., Kuokkala, V.T., 2010. Dependence of tensile deformation behavior of TWIP steels on stacking fault energy, temperature and strain rate. Acta Mater. 58, 5129–5141.

Cowper, G., Symonds, P., 1957. Strain Hardening and Strain-rate Effects in the Impact Loading of Centilevered Beams. Brown University Division of Applied Mathematics, Providence, Rhode Island, USA.

Choi, W.M., Jo, Y.H., Sohn, S.S., Lee, S., Lee, B.J., 2018. Understanding the physical metallurgy of the CoCrFeMnNi high-entropy alloy: an atomistic simulation study. npj Comp. Mater. 4, 1.

Cubuk, E.D., Ivancic, R.J.S., Schoenholz, S.S., Strickland, D.J., Basu, A., Davidson, Z.S., Keim, N.C., 2017. Structure-property relationships from universal signatures of plasticity in disordered solids. Science 358, 1033–1037.

Ding, Z.Y., He, Q.F., Wang, Q., Yang, Y., 2018. Superb strength and high plasticity in laves phase rich eutectic medium-entropy-alloy nanocomposites. Int. J. Plast. 106, 57–72.

Fang, Q., Li, L., Li, J., Wu, H., Huang, Z., Liu, B., Liu, Y., Liaw, P.K., 2019. A statistical theory of probability-dependent precipitation strengthening in metals and alloys. J. Mech. Phys. Solid. 122, 177–189.

Feng, X.B., Zhang, J.Y., Wang, Y.Q., Hou, Z.Q., Wu, K., Liu, G., Sun, J., 2017. Size effects on the mechanical properties of nanocrystalline NbMoTaW refractory high entropy alloy thin films. Int. J. Plast. 95, 264–277.

Fischlschweiger, M., Cailletaud, G., Antretter, T., 2012. A mean-field model for transformation induced plasticity including backstress effects for non-proportional loadings. Int. J. Plast. 37, 53–71.

Gao, M.C., Niu, C., Jiang, C., Irving, D.L., 2016. Applications of special quasi-random structures to high-entropy alloys. In: High-entropy Alloys. Springer, Cham.

Guo, L., Xiao, D., Wu, W., Ni, S., Song, M., 2018. Effect of Fe on microstructure, phase evolution and mechanical properties of $(AlCoCrFeNi)_{100-x}Fe_x$ high entropy alloys processed by spark plasma sintering. Intermetallics 103, 1–11.

Ghassemi-Armaki, H., Maaß, R., Bhat, S.P., Sriram, S., Greer, J.R., Kumar, K.S., 2014. Deformation response of ferrite and martensite in a dual-phase steel. Acta Mater. 62, 197–211.

Ghassemi-Armaki, H., Leff, A.C., Taheri, M.L., Dahal, J., Kamarajugadda, M., Kumar, K.S., 2017. Cyclic compression response of micropillars extracted from textured nanocrystalline NiTi thin-walled tubes. Acta Mater. 136, 134–147.

Grässel, O., Krüger, L., Frommeyer, G., Meyer, L.W., 2000. High strength Fe–Mn–(Al, Si) TRIP/TWIP steels development—properties—application. Int. J. Plast. 16, 1391–1409.

Han, J., Kang, S.H., Lee, S.J., Kawasaki, M., Lee, H.J., Ponge, D., Lee, Y.K., 2017. Superplasticity in a lean Fe-Mn-Al steel. Nat. Commun. 8, 751.

Hill, R., 1952. The elastic behaviour of a crystalline aggregate. Proc. Phys. Soc. Lond. 65, 349–354.

Huang, L., Lin, W., Lin, B., Liu, F., 2016. Exploring the concurrence of phase transition and grain growth in nanostructured alloy. Acta Mater. 118, 306–316.

Huang, S., Huang, H., Li, W., Kim, D., Lu, S., Li, X., Holmström, E., Kwon, S.K., Vitos, L., 2018. Twinning in metastable high-entropy alloys. Nat. Commun. 9, 2381.

Jha, S.K., Szczepanski, C.J., John, R., Larsen, J.M., 2015. Deformation heterogeneities and their role in life-limiting fatigue failures in a two-phase titanium alloy. Acta Mater. 82, 378–395.

Ji, W., Wang, W., Wang, H., Zhang, J., Wang, Y., Zhang, F., 2015. Alloying behavior and novel properties of cocrfenimn high-entropy alloy fabricated by mechanical alloying and spark plasma sintering. Intermetallics 56, 24–27.

Javanbakht, M., Levitas, V.I., 2015. Interaction between phase transformations and dislocations at the nanoscale. Part 2: phase field simulation examples. J. Mech. Phys. Solid. 82, 164–185.

Javanbakht, M., Levitas, V.I., 2016. Phase field simulations of plastic strain-induced phase transformations under high pressure and large shear. Phys. Rev. B 94, 214104.

Kadkhodapour, J., Butz, A., Ziaei-Rad, S., Schmauder, S., 2011. A micro mechanical study on failure initiation of dual phase steels under tension using single crystal plasticity model. Int. J. Plast. 27, 1103–1125.

Khan, A.S., Pandey, A., Gnäupel-Herold, T., Mishra, R.K., 2011. Mechanical response and texture evolution of AZ31 alloy at large strains for different strain rates and temperatures. Int. J. Plast. 27 (5), 688–706.

Kim, J.H., Kim, D., Barlat, F., Lee, M.G., 2012. Crystal plasticity approach for predicting the Bauschinger effect in dual-phase steels. Mater. Sci. Eng. 539, 259–270.
Kim, S.H., Kim, H., Kim, N.J., 2015. Brittle intermetallic compound makes ultrastrong low-density steel with large ductility. Nature 518, 77–79.
Landau, L.D., Lifshitz, E.M., 1999. Theory of Elasticity, third ed. Butterworth-Heinemann, Oxford.
Lee, M.G., Kim, S.J., Han, H.N., Jeong, W.C., 2009. Implicit finite element formulations for multi-phase transformation in high carbon steel. Int. J. Plast. 25, 1726–1758.
Levitas, V.I., Javanbakht, M., 2015a. Thermodynamically consistent phase field approach to dislocation evolution at small and large strains. J. Mech. Phys. Solid. 82, 345–366.
Levitas, V.I., Javanbakht, M., 2015b. Interaction between phase transformations and dislocations at the nanoscale. Part 1. General phase field approach. J. Mech. Phys. Solid. 82, 287–319.
Li, X., Lu, K., 2017. Playing with defects in metals. Nat. Mater. 16, 700.
Li, X., Wei, Y., Lu, L., Lu, K., Gao, H., 2010. Dislocation nucleation governed softening and maximum strength in nano-twinned metals. Nature 464, 877.
Li, Z., Pradeep, K.G., Deng, Y., Raabe, D., Tasan, C.C., 2016. Metastable high-entropy dual-phase alloys overcome the strength–ductility trade-off. Nature 534, 227.
Li, Z., Körmann, F., Grabowski, B., Neugebauer, J., Raabe, D., 2017a. Ab initio, assisted design of quinary dual-phase high-entropy alloys with transformation-induced plasticity. Acta Mater. 136, 262–270.
Li, Z., Tasan, C.C., Pradeep, K.G., Raabe, D., 2017b. A TRIP-assisted dual-phase high-entropy alloy: grain size and phase fraction effects on deformation behavior. Acta Mater. 131, 323–335.
Li, Z., Raabe, D., 2017. Influence of compositional inhomogeneity on mechanical behavior of an interstitial dual-phase high-entropy alloy. Mater. Chem. Phys. 210, 29–36.
Li, J., Fang, Q.H., Liu, B., Liu, Y., 2018. Transformation induced softening and plasticity in high entropy alloys. Acta Mater. 147, 35–41.
Liu, S., Wei, Y., 2017. The Gaussian distribution of lattice size and atomic level heterogeneity in high entropy alloys. Ext. Mech. Lett. 11, 84–88.
Liang, Y.J., Wang, L., Wen, Y., Cheng, B., Wu, Q., Cao, T., Xiao, Q., Xue, Y.F., Sha, G., Wang, Y.D., Ren, Y., Li, X.Y., Wang, L., Wang, F.C., Cai, H.N., 2018. High-content ductile coherent nanoprecipitates achieve ultrastrong high-entropy alloys. Nat. Commun. 9 (1), 4063.
Lu, K., Lu, L., Suresh, S., 2009. Strengthening materials by engineering coherent internal boundaries at the nanoscale. Science 324, 349–352.
Lu, W., Liebscher, C.H., Dehm, G., Raabe, D., Li, Z., 2018. Bidirectional transformation enables hierarchical nanolaminate dual-phase high-entropy alloys. Adv. Mater., 1804727.
Ma, D., Grabowski, B., Körmann, F., Neugebauer, J., Raabe, D., 2015. Ab initio thermodynamics of the CoCrFeMnNi high entropy alloy: importance of entropy contributions beyond the configurational one. Acta Mater. 100, 90–97.
Mahnken, R., Wolff, M., Schneidt, A., Böhm, M., 2012. Multi-phase transformations at large strains–Thermodynamic framework and simulation. Int. J. Plast. 39, 1–26.
Ming, K., Bi, X., Wang, J., 2018. Realizing strength-ductility combination of coarse-grained $Al_{0.2}Co_{1.5}CrFeNi_{1.5}Ti_{0.3}$ alloy via nano-sized, coherent precipitates. Int. J. Plast. 100, 177–191.
Maier-Kiener, V., Schuh, B., George, E.P., Clemens, H., Hohenwarter, A., 2017. Nanoindentation testing as a powerful screening tool for assessing phase stability of nanocrystalline high-entropy alloys. Mater. Des. 115, 479–485.
Niu, C., LaRosa, C.R., Miao, J., Mills, M.J., Ghazisaeidi, M., 2018. Magnetically-driven phase transformation strengthening in high entropy alloys. Nat. Commun. 9, 1363.
Norfleet, D.M., Sarosi, P.M., Manchiraju, S., Wagner, M.X., Uchic, M.D., Anderson, P.M., Mills, M.J., 2009. Transformation-induced plasticity during pseudoelastic deformation in Ni–Ti microcrystals. Acta Mater. 57, 3549–3561.
Olson, G.B., Cohen, M., 1976. Nucleation: Part I. General concepts and the FCC→ HCP transformation. Metall. Trans. 7, 1897–1904.
Plimpton, S., 1993. Fast parallel algorithms for short-range molecular dynamics. J. Comput. Phys. 117, 1–19.
Pogrebnjak, A.D., Yakushchenko, I.V., Bondar, O.V., Beresnev, V.M., Oyoshi, K., Ivasishin, O.M., Amekura, H., Yoshihiko, T., Opielak, M., Kozak, C., 2016. Irradiation resistance, microstructure and mechanical properties of nanostructured (TiZrHfVNbTa) N coatings. J. Alloy. Comp. 679, 155–163.
Ramazani, A., Mukherjee, K., Schwedt, A., Goravanchi, P., Prahl, U., Bleck, W., 2013. Quantification of the effect of transformation-induced geometrically necessary dislocations on the flow-curve modelling of dual-phase steels. Int. J. Plast. 43, 128–152.
Song, R., Wei, L., Yang, C., Wu, S., 2018. Phase formation and strengthening mechanisms in a dual-phase nanocrystalline CrMnFeVTi high-entropy alloy with ultrahigh hardness. J. Alloy. Comp. 744, 552–560.
Stukowski, A., 2012. Visualization and analysis of atomistic simulation data with ovito-the open visualization tool. Model. Simul. Mater. Sci. 1, 15012.
Svanidze, E., Besara, T., Ozaydin, M.F., Tiwary, C.S., Wang, J.K., Radhakrishnan, S., Siegrist, T., 2016. High hardness in the biocompatible intermetallic compound β-Ti3Au. Sci. Adv. 2, 1600319.
Santodonato, L.J., Zhang, Y., Feygenson, M., Parish, C.M., Gao, M.C., Weber, R.J., Liaw, P.K., 2015. Deviation from high-entropy configurations in the atomic distributions of a multi-principal-element alloy. Nat. Commun. 6, 5964.
Tasan, C.C., Hoefnagels, J.P., Diehl, M., Yan, D., Roters, F., Raabe, D., 2014. Strain localization and damage in dual phase steels investigated by coupled in-situ deformation experiments and crystal plasticity simulations. Int. J. Plast. 63, 198–210.
Tao, W., Cao, P., Park, H.S., 2018. Atomistic simulation of the rate-dependent ductile-to-brittle failure transition in bicrystalline metal nanowires. Nano Lett. 18, 1296–1304.
Tang, Z., Yuan, T., Tsai, C.W., Yeh, J.W., Lundin, C.D., Liaw, P.K., 2015. Fatigue behavior of a wrought Al0.5CoCrCuFeNi two-phase high-entropy alloy. Acta Mater. 99, 247–258.
Tracy, C.L., Park, S., Rittman, D.R., Zinkle, S.J., Bei, H., Lang, M., Ewing, R.C., Mao, W.L., 2017. High pressure synthesis of a hexagonal close-packed phase of the high-entropy alloy CrMnFeCoNi. Nat. Commun. 8, 15634.
Wang, L., Guan, P., Teng, J., Liu, P., Chen, D., Xie, W., Ma, E., 2017. New twinning route in face-centered cubic nanocrystalline metals. Nat. Commun. 8, 2142.
Wang, J., Zeng, Z., Weinberger, C.R., Zhang, Z., Zhu, T., Mao, S.X., 2015a. In situ atomic-scale observation of twinning-dominated deformation in nanoscale body-centred cubic tungsten. Nat. Mater. 14, 594.
Wang, Z., Qu, R.T., Scudino, S., Sun, B.A., Prashanth, K.G., Louzguine-Luzgin, D.V., Eckert, J., 2015b. A novel method to achieve grain refinement in aluminum. NPG Asia Mater. 7, 229.
Wang, Y., Liu, B., Yan, K., Wang, M., Kabra, S., Chiu, Y.L., Dye, D., Lee, P.D., Liu, Y., Cai, B., 2018. Probing deformation mechanisms of a FeCoCrNi high-entropy alloy at 293 and 77 K using in situ neutron diffraction. Acta Mater. 154, 79–89.
Widom, M., Gao, M.C., Yeh, J.W., Liaw, P.K., Zhang, Y., 2016. High-entropy Alloys: Fundamentals and Applications. Springer International Publishing, pp. P348–P351.
Wu, Y., Bönisch, M., Alkan, S., Abuzaid, W., Sehitoglu, H., 2018. Experimental determination of latent hardening coefficients in FeMnNiCoCr. Int. J. Plast. 105, 239–260.
Wu, G., Chan, K.C., Zhu, L., Sun, L., Lu, J., 2017. Dual-phase nanostructuring as a route to high-strength magnesium alloys. Nature 545, 80.
Xu, W., Birbilis, N., Sha, G., Wang, Y., Daniels, J.E., Xiao, Y., Ferry, M., 2015. A high-specific-strength and corrosion-resistant magnesium alloy. Nat. Mater. 14, 1229.
Xie, G.M., Ma, Z.Y., Geng, L., 2009. Partial recrystallization in the nugget zone of friction stir welded dual-phase Cu–Zn alloy. Phil. Mag. 89, 1505–1516.
Yamakov, V., Wolf, D., Phillpot, S.R., Mukherjee, A.K., Gleiter, H., 2004. Deformation-mechanism map for nanocrystalline metals by molecular-dynamics simulation. Nat. Mater. 3, 43.
Yu, C., Kang, G., Kan, Q., 2018. A micromechanical constitutive model for grain size dependent thermo-mechanically coupled inelastic deformation of super-elastic NiTi shape memory alloy. Int. J. Plast. 105, 99–127.
Yu, Q., Shan, Z.W., Li, J., Huang, X., Xiao, L., Sun, J., Ma, E., 2010. Strong crystal size effect on deformation twinning. Nature 463, 335.
Yeh, J.W., Chen, S.K., Lin, S.J., Gan, J.Y., Chin, T.S., Shun, T.T., Chang, S.Y., 2004. Nanostructured high-entropy alloys with multiple principal elements: novel alloy design concepts and outcomes. Adv. Eng. Mater. 6 (5), 299–303.
Zhao, S., Stocks, G.M., Zhang, Y., 2017. Stacking fault energies of face-centered cubic concentrated solid solution alloys. Acta Mater. 134, 334–345.
Zhang, Y.H., Zhuang, Y., Hu, A., Kai, J.J., Liu, C.T., 2017a. The origin of negative stacking fault energies and nano-twin formation in face-centered cubic high entropy

alloys. Scripta Mater. 130, 96–99.

Zhang, F., Wu, Y., Lou, H., Zeng, Z., Prakapenka, V.B., Greenberg, E., Ren, Y., Yan, J.Y., Okasinski, J.S., Liu, X.J., Liu, Y., Zeng, Q.S., Lu, Z.P., 2017b. Polymorphism in a high-entropy alloy. Nat. Commun. 8, 15687.

Zhang, Y., Zuo, T.T., Tang, Z., Gao, M.C., Dahmen, K.A., Liaw, P.K., Lu, Z.P., 2014. Microstructures and properties of high-entropy alloys. Prog. Mater. Sci. 61, 1–93.

Zhu, Y.T., Liao, X.Z., Wu, X.L., 2012. Deformation twinning in nanocrystalline materials. Prog. Mater. Sci. 57, 1–62.

Zheng, Z., Waheed, S., Balint, D.S., Dunne, F.P., 2018. Slip transfer across phase boundaries in dual phase titanium alloys and the effect on strain rate sensitivity. Int. J. Plast. 104, 23–38.

Zheng, S., Beyerlein, I.J., Carpenter, J.S., Kang, K., Wang, J., Han, W., Mara, N.A., 2013. High-strength and thermally stable bulk nanolayered composites due to twin-induced interfaces. Nat. Commun. 4, 1696.